Structural Analysis of Poly(trimethylene terephthalate) Fibers and Films Using Polarized Raman Spectroscopy

Simon Frisk,[†] Richard M. Ikeda,[†] D. Bruce Chase,[‡] Alan Kennedy,[‡] and John F. Rabolt*[,†]

Department of Materials Science and Engineering, University of Delaware, Newark, Delaware 19711, and Central Research and Development, E. I. DuPont de Nemours & Company Inc., Wilmington, Delaware 19880

Received April 20, 2004; Revised Manuscript Received May 16, 2004

ABSTRACT: The evolution of the morphology of poly(trimethylene terephthalate) (PTT) samples subjected to different processing conditions was studied using polarized Raman spectroscopy. Three films (amorphous, hot drawn, and crystalline) were used to determine the structural origin of the vibrational bands in the Raman spectra. The findings were applied to a series of melt-spun PTT fibers. A unique combination of quantitative and spectral analyses was successfully used to gain a better understanding of the structural changes in the samples as the birefringence or density of the sample increases. The determination of the average molecular orientation and the distribution of molecular orientations were combined with a detailed analysis of the evolution of the spectral components of the carbonyl stretching vibration. It was determined that an oriented noncrystalline phase was formed in the samples having low densities (low birefringence). Once a certain degree of molecular order is attained, sudden crystallization can occur for a significant fraction of the oriented molecules. Finally, the density gradually increases due to a simultaneous growth of the oriented noncrystalline and crystalline phases. The findings yield valuable information with respect to the evolution of the sample morphology during spinning of PTT fibers and contribute to the fundamental understanding of fiber processing.

Introduction

Poly(ethylene terephthalate) (PET) and poly(butylene terephthalate) (PBT) have long commercial histories while interest in poly(trimethylene terephthalate) (PTT) has developed only recently because of the discovery of a more economical synthesis of propylene diol. The expanding number of studies on PTT has resulted in a rapid determination of both its chemical and physical properties.[1−29] So far, the greatest interest in PTT comes from the textile industry due to the resilience and elastic recovery of PTT fibers along with superior dyeing ability. DuPont and Shell Chemicals have recently commercialized poly(trimethylene terephthalate), derived from 1,3-propanediol, under the trade names Sorona and Corterra, respectively. The diol component of this polymer, 1,3-propanediol, has been demonstrated to be manufacturable via a biological (fermentation) process from corn sugar. Inevitably, PTT will be used for other applications, especially as characterization studies continue and the cost of production is further decreased.

As in any material, the macroscopic properties of PTT are dependent on its molecular structure. In turn, the structure is the result of the chemical composition of the material and its response to the myriad of processing conditions. Multiple research groups[4,5,21] have shown that the structure of PTT is very different from that of PET and PBT, although their chemical composition is very similar. The propylene glycol segment of PTT adopts a *trans−gauche−gauche−trans* (*tggt*) conformation in the crystalline phase, and the unit cell contains two monomer units forming a 2/1 helix (as seen in Figure 1a). The consecutive phenyl groups along the chain are inclined in opposite directions. The angle formed by the normal to the terephthaloyl residue with respect to the long axis has been determined to be 52°.[4] In contrast, in PET, the ethylene glycol segment adopts the *all-trans* conformation, and successive phenyl groups are oriented in the same direction, resulting in a unit cell containing a single monomer unit. Two crystalline forms of PBT exist, both having phenyl groups in the same direction and only one repeat unit per unit cell.

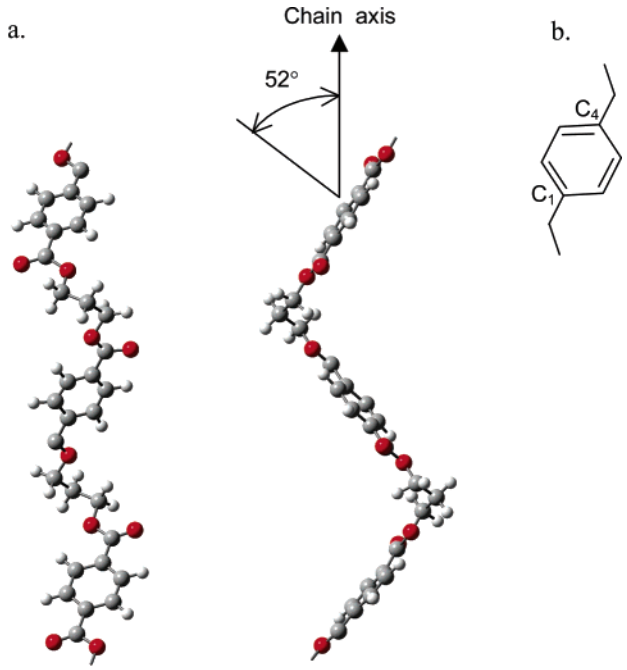

Figure 1. (a) Schematic of part of a PTT molecule in the crystalline phase (*tggt* conformation). (b) Position of the 1 and 4 carbon atoms in the para-disubstituted benzene ring.

[†] University of Delaware.
[‡] DuPont Central Research and Development.
* To whom correspondence should be addressed. E-mail: Rabolt@udel.edu.

10.1021/ma049234j CCC: $27.50 © 2004 American Chemical Society
Published on Web 07/16/2004

The flexible segment of PBT adopts either the *all-trans* or a *gauche−gauche−trans−gauche−gauche* conformation. The most probable conformations of the *m*-methylene glycol segment in the amorphous phase are *tgt*, *tgg*, and *ttt* for PET and *gttg* for PTT. Many conformations exist in the amorphous phase of PBT. It has been shown that these structural differences are the main source of the difference in physical properties between these three polymers.[2]

Most structural studies on PTT have been limited to the determination of average quantities (i.e., birefringence, tensile modulus, etc.) or to studies of specific phases (e.g., crystal studies by X-ray). Vibrational spectroscopy allows researchers to gain insights into the structure of the different molecular phases. Information about the structure and orientation of both the crystalline and the amorphous phases of the material can be obtained. Infrared spectroscopy has been used to study chain conformation and orientation in PTT.[3,7,13] Only two groups have studied PTT using polarized Raman spectroscopy. These studies date back to 1977 and 1986. Ward and Wilding[3] observed and compared conformational changes in different PET, PTT, and PBT samples while Bulkin et al.[6,7] studied crystallization kinetics and conformational reorganization based on a particular vibration in the Raman spectrum of PTT. Recent theoretical and instrumental developments in polarized Raman spectroscopy have allowed the gain of more detailed information about the structure and orientation in the different molecular phases.[30−33] On the basis of the detailed analysis of polarized Raman scattering by Bower,[34] different methods for determining the second and fourth coefficient of the molecular orientation distribution have been developed.[30,31,35,36] The pros and cons of these methods were discussed in a previous publication.[37] In addition, a procedure to obtain orientation-insensitive spectra from a series of standard polarized Raman spectra was developed Frisk et al.[38] This allowed an easy determination of the dependence of different spectral features on the sample structure.

This publication describes a detailed spectral analysis of PTT. Initially, a better understanding of the origin of the bands in the Raman spectra was achieved by a study of three PTT films: amorphous, hot drawn, and crystalline. The findings served as a basis for the analysis of a series of polarized Raman measurements obtained on different PTT fibers. Finally, the degree of molecular orientation and the shape of the distribution of orientations were determined in order to gain a better understanding of the evolution of the structure with changing processing conditions.

Theory. Raman scattering is a two-photon process involving a total of four possible polarization vectors: two for the incoming radiation and two for the scattered light. The analysis of polarized Raman spectra requires one to relate two coordinate systems in order to deduce information regarding the average degree of molecular orientation. The laboratory frame of reference defines the directionality of the different measurements, whereas the molecular frame of reference defines the directionality of the molecular vibrations. These two sets of coordinate axes are related by a complex theoretical development, which results in the possibility of determining the orientation distribution function.

Orientation Determination using Polarized Raman Spectroscopy. Bower first developed the explicit theoretical treatment and procedure to determine molecular orientation in samples having uniaxial symmetry by polarized Raman spectroscopy.[39] Various research groups[30,31,33] related the theoretical expressions determined by Bower to experimental quantities obtained by employing a combination of different source and scattering polarization directions and sample orientation. These procedures can be used to determine five independent quantities, which include the second- and fourth-order coefficients of the orientation distribution function, $\langle P_2(\cos\theta)\rangle$ and $\langle P_4(\cos\theta)\rangle$, respectively. These will be referred to P_2 and P_4, and their significance is briefly discussed below. The other quantities experimentally determined (a_1, a_2, and b) are directly dependent on the three principal axes of the polarizability tensor (α_1, α_2, and α_3) of the particular vibration being studied.

As previously mentioned, the conformational states of the flexible segment in the three polyesters (PET, PTT, and PBT) are very different. Thus, the study of the conformation-sensitive bands should allow a direct observation of structural differences. Unfortunately, the majority of these conformation-sensitive bands have very small Raman scattering cross sections, resulting in low scattering intensities. In addition, these bands are usually not isolated in the spectrum, making the analysis very complex. Finally, the quantitative determination of the degree of orientation requires the knowledge of the orientation of the principal tensor elements with respect to the molecular chain. For those two reasons, our quantitative orientation studies are based on the C_1-C_4 benzene ring (Figure 1b) stretching vibration for which Lewis and Bower[40] determined that the axis associated with α_3 corresponds, to a close approximation, to the C_1-C_4 axis of the ring. The corresponding peak in the Raman spectra is isolated and very intense and appears at 1614 cm^{-1}. Recently, Frisk et al.[38] compared different methods to determine P_2, P_4, a_1, a_2, and b. The results presented in this publication were determined utilizing the most complete method, for which the only assumption is uniaxial symmetry in the samples.

Orientation Distribution Function. The purpose of determining P_2 and P_4 is to quantify the average degree of orientation of the molecules in a sample and to define the distribution of orientations around the mean. Mathematically, the orientation distribution function (ODF) is described by a series expansion of a function $N(\theta)$ in terms of Legendre polynomials in cos θ. For a uniaxial system, the function $N(\theta)$ is defined such that the fraction of units oriented within the solid angle sin θ dθ at an angle θ to the unique axis of the system can be represented by $N(\theta)$ sin θ dθ. The expansion coefficients of the Legendre polynomial represent the value of $P_l(\cos\theta)$ averaged over the all the units of the distribution and are usually defined as $\langle P_l(\cos\theta)\rangle$. Practically, the number of coefficients that one can determine will depend on the characterization technique being used. Many techniques, as for example infrared spectroscopy, allow the determination of only the first nonzero P coefficient (aka P_2). Unfortunately, knowledge of P_2 gives only a measure of the average orientation angle of the molecules. To gain a better understanding of molecular distribution, the shape of the ODF must be defined (i.e., many different distributions can result in the same P_2 value). It was shown[34] that polarized Raman spectroscopy allows the determination of P_2 and P_4 (the first two nonzero terms), which

narrows the range of possible distributions. Theoretically, an infinite number of coefficients are needed to fully define the ODF.

To better understand the significance of P_2 and especially P_4 with respect to the molecular orientation distribution, one needs a graphical representation of the ODF. Bower[41] and Pottel et al.[42] developed a mathematical method to determine the most probable distribution function ($N_{mp}(\theta)$) based on the experimentally determined P_l values. Their method is based on maximum information entropy statistics, which results in a function of the form

$$N_{mp}(\theta) = \exp\{\sum_l \lambda_l P_l(\cos\theta)\} \quad (1)$$

where the λ_l are Lagrange multipliers, which must be chosen to satisfy the following constraint:

$$P_l = \langle P_l(\cos\theta)\rangle = \int_0^{\pi} N_{mp}(\theta) P_l(\cos\theta)\sin\theta\, d\theta \quad (2)$$

The $P_l(\cos\theta)$ terms represent the Legendre polynomial, of which the first two nonzero terms are

$$P_2 = \frac{1}{2}(3\langle\cos^2\theta\rangle - 1) \quad (3a)$$

$$P_4 = \frac{1}{8}(3 - 30\langle\cos^2\theta\rangle + 35\langle\cos^4\theta\rangle) \quad (3b)$$

Yang and Michielsen[43] showed that one can solve for $N_{mp}(\theta)$ by varying the λ_l in order to minimize the sum:

$$(P_2^{fit} - P_2^{exp})^2 + (P_4^{fit} - P_4^{exp})^2 \quad (4)$$

where P_l^{fit} are obtained for eqs 3 and P_l^{exp} are the values determined experimentally. The most probable ODF can be plotted for each set of orientation coefficients, which permits the visualization of the evolution of the molecular orientation and distribution in a series of samples.

Orientation-Insensitive Spectra. A method has been developed by Frisk et al.[38] to mathematically construct a Raman spectrum that is invariant under the operation of rotation. The purpose of this development is to separate the quantitative information about the number of oscillators present in various phases from the information related to their orientation. By adding the specific polarized Raman spectra, as defined in eq 5, one obtains a spectrum that is representative of the different phases in the sample and completely independent of the degree of molecular orientation.

$$I_{zz} + 2I_{yy} + 4I_{yz} + 2I_{yx} = C \quad (5)$$

where C is a term that can be determined from measurements made on an isotropic sample. The I_{ij} represent the band intensities obtained for specific polarizations of the incoming and scattered light (defined in the Experimental Method section). The construction of this orientation-insensitive spectrum can greatly contribute to the understanding of the evolution of different phases in a series of samples having the same chemical structure but that have been subject to different processing conditions. For example, the interpretation of the evolution of the different components of a complex band determined by curve fitting could more easily be interpreted as a function of the characteristic conformations of the different phases. The construct spectrum can also facilitate the assignment of unknown spectral peaks by eliminating the effect of orientation on band shapes and intensities.

Experimental Section

Materials. Three PTT films were studied. The first was a completely amorphous film ~270 μm thick, which was named Am-film. The isotropic nature of the film was verified by measuring a depolarization ratio for the 1614 cm^{-1} band of 0.52 ± 0.03 for three different experimental geometries: film normal to the incident radiation, film normal to the incident radiation but rotated 30° around that axis, and film tilted ~45° with respect to the incident radiation. The second film was created by drawing a 1.5 cm wide strip of the amorphous film over a hot plate (set temperature: 150 °C). The film, subjected to a high static tensile force, was slowly lowered over the hot plate. Once the glass transition temperature was reached (T_g ~ 40 °C), the film was manually stretched to the maximum strain in less than 1 s and immediately placed in an ice−water bath. The resulting draw ratio (~3×) indicated the possibility of a relatively high degree of molecular orientation. Also, the combination of high molecular orientation and heat is expected to induce a certain amount of crystallinity in the sample.[10,14] The central section of the drawn film (necked region) was cut and used for all the measurements. This film is referred to as Dr-film. The "unidirectional" nature of this film was examined by determining the ratio of the Raman intensities collected with the polarizer and analyzer parallel and then normal to the long axis of the sample, respectively (i.e., ratio = I_{zz}/I_{yy}). The ratio was determined with the sample normal to the incident radiation and with the sample rotated ~45° around the long axis. The two ratios obtained were different by about 20%. Thus, the assumption of unidirectional symmetry in the drawn sample can only be made with caution. The last film being studied was created by heating a ~3 cm^2 piece of isotropic film on a hot plate at 200 °C, which is close to the melting temperature (T_m ~ 230 °C), for 3 h. To minimize the amount of deformation during the crystallization process, the film was constrained between two microscope glass slides by a heavy weight. This film is referred to as the Cr-film. This film is expected to have a high degree of crystallinity with no overall preferred molecular orientation. Approximations of the density of the samples were made by precisely measuring the physical dimensions of the samples and determining their mass on a precision scale (Mettler Toledo). The apparent degree of crystallinity of the samples was calculated assuming on a two-phase system. The percent crystallinity by weight was determined from the specific volume (V) of each sample using the following relationship:

$$\text{wt \% cryst} = (m_{cr}/m_{sample}) \times 100 = ((V_{sample} - V_{am})/(V_{cr} - V_{am})) \times 100 \quad (6)$$

where $V_{am} = 1/\rho_{am}$, $V_{cr} = 1/\rho_{cr}$, and $V_{sample} = 1/\rho_{sample}$ and ρ_{am} corresponds to the density of a fully amorphous sample (1.3067 g/cm^3),[16] ρ_{cr} to the density of a 100% crystalline sample (1.4412 g/cm^3),[16] and ρ_{sample} to the density of our sample. The density calculated for the Am-film (1.31 g/cm^3, ~0 wt % crystallinity) was compared with the value found in the literature (1.3067 g/cm^3)[16] to confirm the accuracy of our method. The densities for the Cr-film and the Dr-film were calculated to be 1.383 g/cm^3 (59 wt % cryst) and 1.333 g/cm^3 (21 wt % cryst), respectively. The density of the Dr-film is expected to be much less accurate because the physical dimensions of the sample were much smaller than for the other two samples, making accurate dimensional measurements difficult.

The second set of samples being studied was a series of melt-spun PTT fibers. The fibers were spun at speeds ranging from 846 to 4150 m/min and were not subject to any postprocess draw. Table 1 lists the seven samples and their respective wind-up speed, density, and birefringence. The apparent degree of crystallinity is also listed.

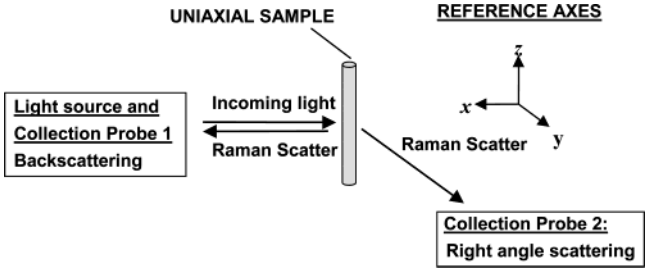

Figure 2. Schematic of the geometry of the experimental setup showing the orientation of the instrumental frame of reference.

Table 1. Properties and Processing Conditions of the As-Spun and Drawn PTT Fibers

sample	spin speed (m/min)	density (g/cm^3)	apparent % crystal	birefringence	draw ratio	draw temp (°C)
fiber-1	846	1.314	5.4	0.010		
fiber-2	1200	1.315	6.2	0.019		
fiber-3	1800	1.316	6.9	0.036		
fiber-4	2600	1.319	9.1	0.044		
fiber-5	2650	1.32	9.9	0.044		
fiber-6	3650	1.322	11.4	0.060		
fiber-7	4150	1.323	12.1	0.063		
fiber-D1	1600	1.328	15.6		2.00	90
fiber-D2	1600	1.332	18.5		2.00	144
fiber-D3	1600	1.345	28.8		1.87	170

Finally, three PTT fibers spun at 1600 m/min and subjected to postprocess draw were studied. Their density and corresponding processing conditions are also listed in Table 1.

Methods. Raman measurements were made using a Holoprobe system (Kaiser Optical Systems Inc.) with a liquid nitrogen cooled CCD detector (Princeton Instruments, Inc.). Two probes with motorized polarizers allowed the simultaneous collection of the backscattering and the right angle scattering for the different polarizations. A frequency-doubled Nd:YAG laser (Coherent, Inc.) was used to pump a Ti:sapphire tunable laser (Spectra-Physics Inc.) tuned to 785 nm, producing a laser power stabilized between 80 and 100 mW. The data were collected using the WinSpec32 software (Princeton Instruments, Inc.) and analyzed using Grams/AI (Thermo-Galactic, Inc.). The collected spectra have a spectral resolution of 4 cm^{-1}. They were subjected to an instrument response function correction using an incandescent white light spectrum. A wavelength calibration was done using a 4-acetamidophenol standard. The spectra were baseline corrected. Finally, experimental uncertainties, such as laser power differences in the two orthogonal polarization directions, were corrected for by using the redundant spectra as described by Lesko et al.[32]

A total of 12 spectra were collected for each sample. Each spectrum corresponds to a specific polarization of the incident and scattered light in the instrumental frame of reference, as defined in Figure 2. A peak intensity labeled I_{zy} represents the scattering intensity of the particular vibration when the incoming and scattered photons are polarized along the *z* and the *y* directions, respectively. Note that the unique axis of the sample (axis 3) coincides with the instrumental *z*-axis. The final four measurements were made in the backscattering mode with the sample rotated ±45° with respect to the *z*-axis (labeled I_{tzz}, I_{tzy}, ...). The five unknown parameters (P_2, P_4, a_1, a_2, and b) were determined by solving a system of five equations[38] using the Excel (Microsoft Corp.) and the Mathematica (Wolfram Research, Inc.) software.

Results and Discussion

Films. The validity of the measurements was verified after processing the polarized Raman spectra for the three films (Am-film, Dr-film, and Cr-film). The fact that there were no observable differences between the *zy* and *yz* spectra (which are theoretically redundant) indicates that the experimental method is adequate. In addition, the perfect overlap of the *zz* and *yy* spectra for the Am-film confirms the in-plane isotropic nature of the sample. The same comparison for the Cr-film shows a small (~10%) intensity difference through the entire spectrum. When the spectral intensities are normalized, the *zz* and *yy* spectra overlap perfectly. This indicates that there are no orientation-induced spectral changes. The overall intensity difference can possibly be attributed to polarization scrambling due to the birefringence of the crystalline phase. For the drawn sample, the overlay of the *zz* and *yy* spectra (without normalization) shows that most bands have different intensities. Only two significant bands (633 and 704 cm^{-1}) appear to overlap. The bands at 848, 950, 1115, 1175, and 1466 cm^{-1} are more intense in the *yy* spectrum, whereas the bands at 910, 1291, 1393, 1411, 1614, and 1717 cm^{-1} are more intense in the *zz* spectrum. These observations indicate that the corresponding vibrations have a preferred orientation, in turn, signifying that the sample is oriented. The evolution of the spectral features as the morphology and orientation changes can be observed when the spectra from the three samples are overlaid on the same plot.

Figures 3 shows the *zz* polarized Raman spectra obtained on the three films. The spectral intensities are normalized at 1614 cm^{-1}. Differences can be observed through the entire spectral range. No peak has the same intensity in the three spectra. The bands at 850 cm^{-1} (ring C−C breathing) and 1116 cm^{-1} (ring C−H in-plane bend or C−O stretch) are identical for the Am-film and the Dr-film. The band at 633 cm^{-1} (ring C−C−C in-plane bend) has the same intensity for the Am-film and the Cr-film. Finally, the bands at 910 cm^{-1} (glycol), 1222 cm^{-1} (CH_2 twist), and 1395 cm^{-1} (complex combination band) are identical for the Dr-film and the Cr-film. The differences observed in the corresponding *yy* spectra (not shown) are not identical to those observed in the *zz* spectra. This indicates that there is a contribution to the peak intensities from the different morphologies and the different degrees of molecular orientation. For example, the difference in the intensity of the band at 1116 cm^{-1} in the *zz* and *yy* polarizations appears to be the same for the amorphous and crystalline samples, whereas the peak intensity for the drawn sample is very different in the two polarizations. The band assignments are mainly based on previous work by Ward and Wilding.[3]

To help determine the origin of the spectral changes, orientation-insensitive spectra[38] for the three samples were constructed (seen in Figure 4) by assuming they have fiber symmetry. Differences in these spectra can only be attributed to changes in molecular morphologies since the contribution of different molecular orientation has been "removed". The bands at 633 and 795 cm^{-1} (ring C−C−C out-of-plane bend) now have the same intensity for the three samples. Most other bands show a systematic increase in intensity. The intensity of the bands at 910, 950, 1115, 1222, 1390, 1470, and 1720 cm^{-1} shows the greatest increase with increasing sample crystallinity. A single band shows the opposite trend. The band at 1410 cm^{-1} (ring C−C stretch) is more intense for the amorphous sample than for the drawn and the crystallized samples. The intensity differences appear to correlate with the varying degrees of crystal-

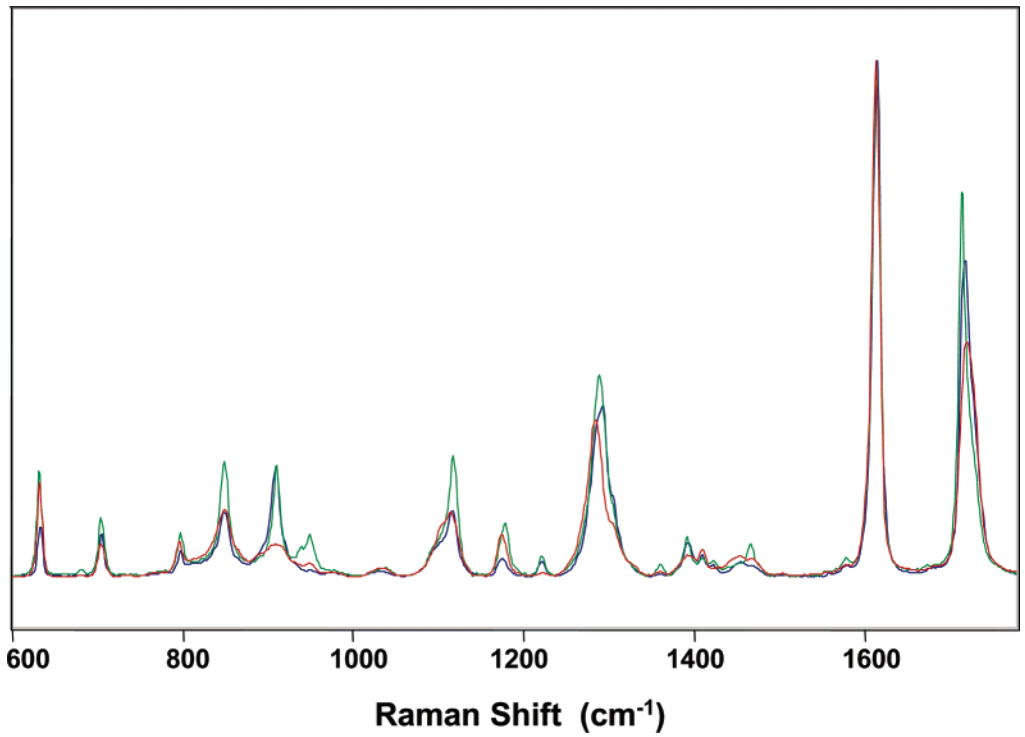

Figure 3. Polarized Raman spectra in the *zz* polarization of the amorphous (red), hot drawn (blue), and crystalline (green) films.

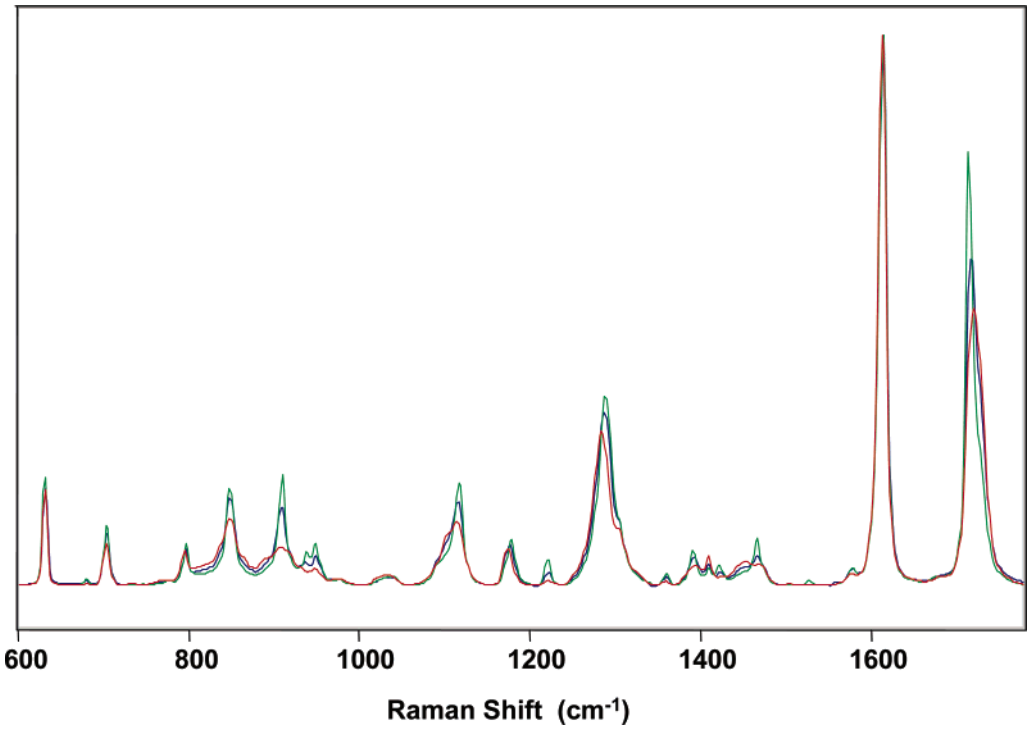

Figure 4. Orientation-insensitive Raman spectra of the amorphous (red), hot drawn (blue), and crystalline (green) films.

linity of the samples, whereas no such correlation could be seen in either the *zz* or *yy* sets of spectra.

A curve-fitting analysis was performed on the orientation-insensitive spectra in order to determine the correlation of the peak intensities, full widths at half the maximum (fwhm), and the total peak area with the sample density. This analysis was performed on the carbonyl stretching vibration following the work by other research groups on PET[44−46] and PTT[7] that has shown that this peak is sensitive to conformational changes. The position of maximum intensity of this peak is shifting, from 1720 cm^{-1} in the amorphous film to 1717 and 1714 cm^{-1} in the hot drawn and the crystallized films, respectively. This confirms the finding of the previous investigation of this multicomponent band of PTT,[7] which has shown a strong dependence of the peak position and the fwhm on the conformational order in the samples. That study also revealed a nonlinear variation of the fwhm as a function of density. In this study, curve fitting was used to separate the different components of the peak in order to better define and understand the origin of the asymmetry in the carbonyl

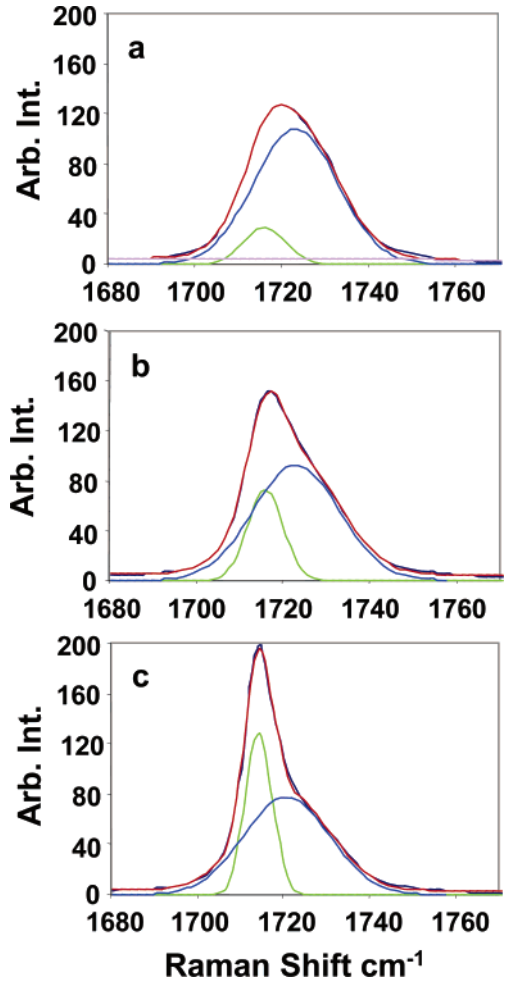

Figure 5. Peak-fitting analysis of the C═O stretch vibration for the amorphous (a), hot drawn (b), and crystallized (c) films: area of the noncrystalline component (blue), area of the crystalline component (green), sum of areas (red), and real data (black).

band in PTT. Two Gaussian peaks were automatically fitted by the Grams software. The residuals were small, and the positions of the two component peaks were the same for the three samples, indicating that the fit was adequate (as seen in Figure 5). The parameters of the fitted component peaks are summarized in Table 2. The area of the two peaks appears to vary linearly with the density as seen in Figure 6. The total area of the carbonyl band is constant as a function of density, indicating that one component band grows at the extent of the other. The decrease in the area of the high-frequency component indicates an overall decrease in the amorphous phase. The constant fwhm indicates that

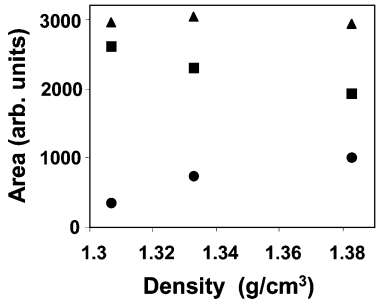

Figure 6. Area of the two components (circles: crystalline; squares: noncrystalline) and the total area (triangles) of the C═O band.

the degree of disorder in this phase remains the same. For the low-frequency component, the increase in the area is the result of an increase in the peak height accompanied by a decrease in the fwhm. The increase in the area reflects a proportional increase in the crystalline phase. The narrowing of the fwhm signifies an ordering of that phase. A similar study of the isolated single component band at 1222 cm^{-1} shows a similar linear increase in intensity with density, as seen in the bottom part of Table 2. The observations made on the film samples help understand the evolution of the morphology in the PTT fibers as the processing conditions are changed.

Fibers. Three constructed orientation-insensitive Raman spectra corresponding to the lowest, a medium, and the highest spin speed fiber samples (fiber-1, fiber-4, and fiber-7, respectively) are plotted in Figure 7. Only three spectra were overlaid in these figures for clarity reasons. The differences in the orientation-insensitive spectra are not as evident as for the film samples, indicating that the morphological structure of the samples are quite similar. The spectra of fiber-1 and fiber-4 are identical, which indicates that either the density difference is too small to result in noticeable spectral changes or the difference in density is not due to an increase in crystallinity. The fiber-7 spectrum shows an increase in the crystalline sensitive peaks, indicating a higher degree of crystallinity. The differences between the three *zz*-polarized spectra (not shown) are much greater and not systematic through the entire spectral range, indicating that the degree of molecular orientation is different in all three samples.

The carbonyl band of the orientation insensitive spectra was curve fitted to observe more precisely the evolution of the structure in the different samples. The curve-fitting routine employed for the films was employed for the fibers. The results are plotted in Figure 8. The fraction of the total area of the component peaks shows an interesting behavior with increasing density.

Table 2. Results of the Peak-Fitting Analysis on the Spectral Bands at 1720 and 1222 cm^{-1} for the Three Film Samples

sample	density (g/cm^3) app % crystal	peak 1 peak 2	height 1 height 2	fwhm 1 fwhm 2	area 1 area 2	height fractions	area fractions	total area
amorph	1.307	1716	29.7	11.1	350	0.22	0.12	2947
	0	1723	108.3	22.5	2597	0.78	0.88	
drawn	~1.333	1716	72	9.6	739	0.44	0.24	3037
	~21	1723	92.8	23.3	2298	0.563	0.76	
cryst	~1.383	1714	129.3	7.3	1010	0.63	0.34	2940
	~59	1721	77.5	23.4	1930	0.37	0.66	

sample	density (g/cm^3)	peak	height	fwhm	area
amorph	1.307	1222	1.8	12.7	24.5
drawn	~1.333	1221	5.8	9.5	58.6
cryst	~1.383	1221	11.4	7.9	95.7

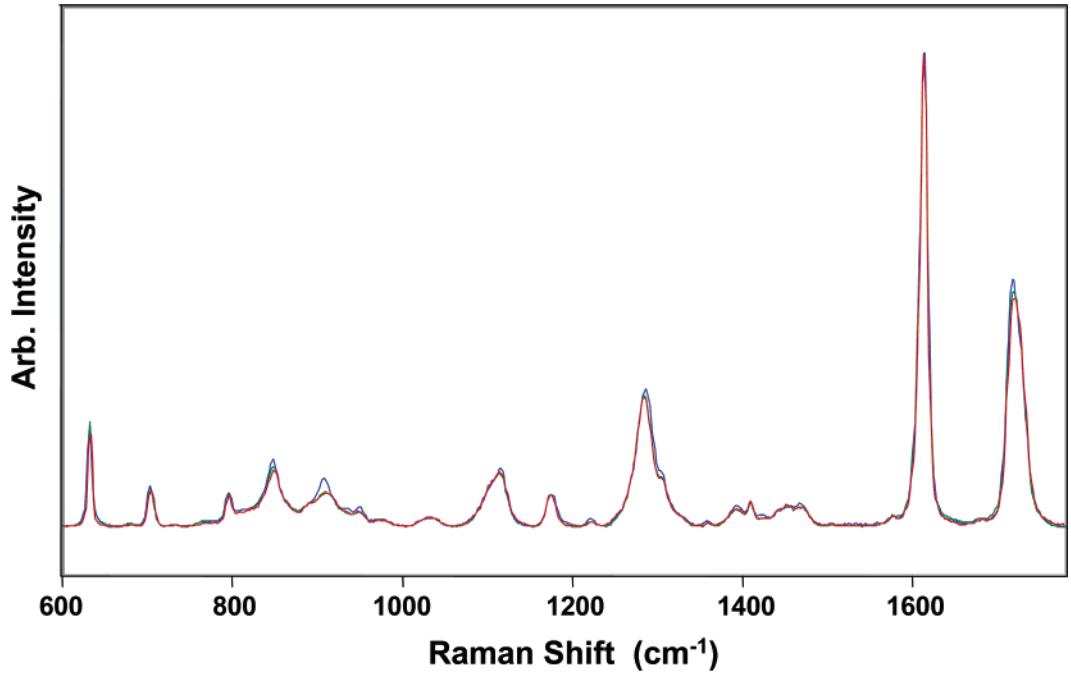

Figure 7. Orientation-insensitive Raman spectra of fiber-1 (red), fiber-4 (green), and fiber-7 (blue).

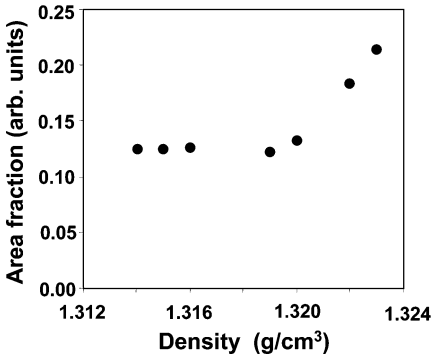

Figure 8. Fraction of the crystalline component of the C═O band obtained from the curve-fitting analysis of the as-spun fibers.

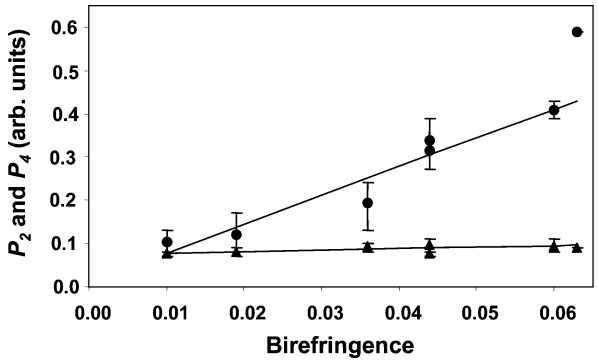

Figure 9. P_2 (circles) and P_4 (triangles) as a function of birefringence for the as-spun PTT fibers. Linear regression for P_2 and P_4 (omitting the last data point)

The curve plotted in Figure 8 shows the area fraction of the low-frequency component peak (representative of the crystalline phase). The curve is constant for sample densities up to approximately 1.319 g/cm^3. It is interesting to note that the constant fraction corresponds exactly to the fraction obtained for the isotropic film. At 1.319 g/cm^3, there is a break in the curve after which the fraction of the total area of the "crystalline" component peak is increasing rapidly with increasing density. The observed trend can be explained by the creation of an oriented noncrystalline phase. Initially (low spin speeds), the amorphous phase is dominant. As the spin speed increases, the molecular orientation increases, resulting in an ordering of the molecules. This ordering initially takes place without the occurrence of crystallization, resulting in the formation of an oriented noncrystalline phase. The conformational changes occurring during the orientation seem to have a minimal effect on the frequency of the C═O stretching vibrations. The more organized noncrystalline phase is denser than the amorphous phase. Once a sufficient degree of order is reached, crystallization is initiated within the more ordered phase. Crystallization can only occur for molecules having a specific registry. It is possible that the regularity of the molecular arrangement in the crystalline phase can cause significant dipole−dipole interaction to occur and thus significantly affect the frequency of the C═O stretching vibration (increasing slope in Figure 8). This analysis justifies the lack of spectral differences in the orientation insensitive spectra of fiber-1 and fiber-4. The creation of an oriented noncrystalline phase should be complemented by an overall increase in the average molecular orientation (P_2).

The P_2 and P_4 values determined for the seven as-spun fibers are plotted as a function of birefringence in Figure 9. Each data point is an average of five measurements made independently on a single filament carefully separated from each yarn. Experimental difficulties related to the measurements made on the tilted fibers and their normalization to the other measurements are believed to be the main source of error when using this method.[38] These difficulties have led in most cases to imaginary solutions when the system of equations is solved for highly birefringent samples. Thus, the data point for a birefringence value of 0.060 is an average of only two measurements. The data point for the highest birefringence is the result of a single successful set of measurements and is therefore used with caution. P_2 appears to increases almost linearly through the entire birefringence range, indicating an

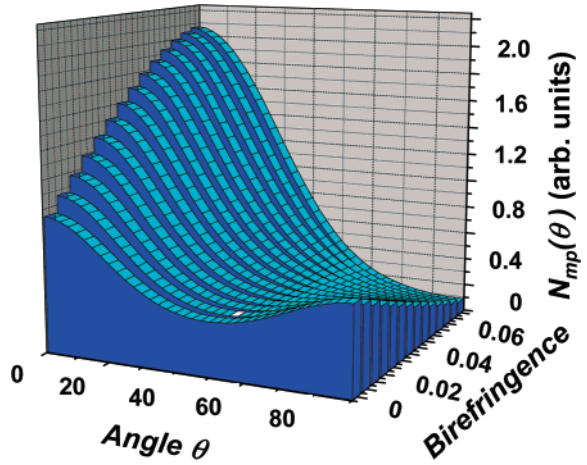

Figure 10. Orientation distribution function as a function of birefringence for the as-spun PTT fibers.

increase in the average orientation of the C_1-C_4 axis of the benzene rings. The observed increase in the average molecular orientation is consistent with the previous observations. P_4 is constant with increasing birefringence. The common belief is that P_4 represents the width of the distribution of orientations around the average value. That would indicate that the distribution of orientations in our samples remains the same as the birefringence is increasing (i.e., as the orientation increases), which may be counterintuitive. These results contrast with results obtained on PET by Lesko et al.[32] Their results showed both increasing P_2 and P_4 values with increasing spin speed (or birefringence). From their spectral analysis, they concluded that an oriented noncrystalline phase was formed at low spin speeds followed by crystallization. The onset of crystallization in PET was evidenced by a break in the P_2 and P_4 curves (slope increase) at some intermediate spin speed (~2600 m/min). Although the results on the PTT samples do not show a similar change in the P_2 and P_4 slopes, the presence of an oriented noncrystalline phase was proven by the previous spectral analysis. The quantitative results support that analysis. The increase in orientation necessary to form an oriented phase is observed for the low-density samples (low birefringence).

To get a clearer picture of the evolution of the ODF, we fit the scattered P_2 and P_4 data with linear functions (Figure 9), which were then used to calculate sets of P_2 and P_4 values for different birefringence values. These were then used to determine and plot the different ODFs. The evolution of the distribution of molecular orientation with increasing spin speed can be seen in Figure 10. At low spin speeds (low birefringence) the distribution is very broad with a preferred orientation (PO) of the benzene ring axis along the fiber axis (0°). The width of the distribution around the preferred direction is increasing at the expense of the 90° direction (perpendicular to the fiber axis) as the sample birefringence increases. This indicates that the molecules gradually oriented themselves along the fiber axis. An increase in the ring orientation along the fiber axis would be expected to increase the sharpness of the ODF. In fact, for the PTT samples, the width of the distribution increased with birefringence. The broadening of the distribution at the expense of an increase in the intensity around the PO for the higher birefringence samples indicates that the preferred inclination of the benzene ring with respect to the unique axis in highly

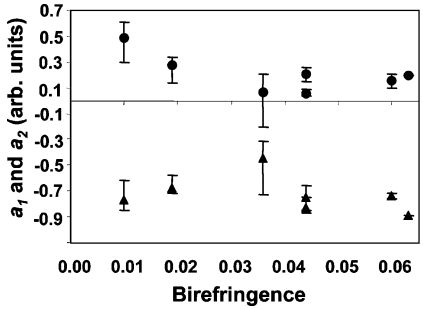

Figure 11. a_1 (circles) and a_2 (triangles) as a function of birefringence for the as-spun PTT fibers.

oriented samples is not 0°. This can be explained by the fact that in the crystalline phase the molecules adopt a *tggt* conformation, resulting in the C_1-C_4 axis of the ring being oriented at 38° from the chain axis (as seen in Figure 1). Thus, the growth of the width of the distribution around the PO may correspond to growth of the crystalline phase at the expense of the amorphous phase. These results concur with the previous observation of the creation of an amorphous oriented phase before significant crystallization occurs.

An attempt to explain the widening of the ODF with increasing birefringence was made based on an extrapolation of the experimental data to a theoretical maximum. For an ideal 100% crystalline sample, all the molecules adopt the same conformation and are oriented in the exact same direction (Figure 1). For such a sample, the density and the theoretical values of P_2 and P_4 can be calculated. Thus, for a benzene ring orientation of 38°, these values are 0.431 and −0.267 for P_2 and P_4, respectively. For these values, the ODF is a delta function positioned at an angle of 38°. Therefore, one can imagine that the widening of the ODFs does represent the increase in crystallinity. Once the degree of crystallinity is significant (i.e., a great number of benzene rings oriented at 38°), the PO of the distribution shifts away from 0°. It shifts more and more toward 38° as the degree of crystallinity increases. This trend was observed for a series of ODFs (not shown) corresponding to theoretically determined P_2 and P_4 values. These values were based on a linear fit between our highest spin speed experimental value and the theoretical maxima.

In addition to P_2 and P_4, solving the system of equations allows the determination of two terms directly dependent on the principal tensor elements of the polarizability. a_1 and a_2 (i.e., $a_1 = \alpha_1/\alpha_3$ and $a_2 = \alpha_2/\alpha_3$) are plotted as a function of birefringence in Figure 11. They are opposite in sign and in their trend. a_1 appears to first decreases exponentially until a birefringence value of approximately 0.035 and then stay constant as the birefringence increases. The trend of a_2 with increasing birefringence is not as clear. The variation of the principal tensor elements with birefringence raises the question regarding their dependence on the local environment. The change in the a_1 (and a_2) behavior seems to coincide with the development of the different phases suggested by the evolution of the ODF's with sample density. The amorphous chains progressively align with their chain axes along the fiber direction while the crystalline phase aligns such as the helices are pointing in the fiber direction. With multiple phases, there is a possibility of averaging polarizability tensor values representative of the fraction of the different phases present in a manner to

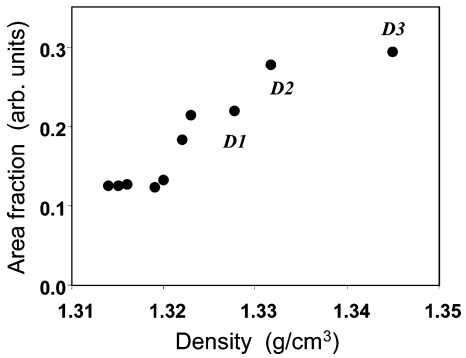

Figure 12. Fraction of the crystalline component of the C═O band obtained from the curve-fitting analysis of the as-spun and the drawn fibers (D1, D2, and D3).

yield "observed" tensor elements that change in some systematic fashion.

Drawn and As-Spun Fibers. A similar spectral analysis was performed on the three fiber samples that were subject to a postprocess draw. The curve-fitting results were combined with those obtained on the fibers in order to observe the evolution of the morphology for higher sample densities. The fraction of the total peak area corresponding to the "crystalline" component peaks is plotted as a function of density in Figure 12. The plot shows three distinct regions. The observed trend for the low- and medium-density samples was explained previously by first the creation of the oriented noncrystalline phase followed by a sudden crystallization. Note that the area fractions obtained for the low-density samples (0.13) correspond to the fractions obtained for the totally isotropic film. The third distinct region (∼1.325 to ∼1.35 g/cm^3) shows that the area fraction of the component peak corresponding to the crystalline phase is still increasing with density but at a much slower rate than in the second region. For the crystallized film (density of ∼1.38 g/cm^3) the area fraction of the "crystalline" component was determined to be 0.34 (Table 2), indicating the possibility that the trend observed for the higher density fibers extends to even higher sample densities. In the first zone, the molecules in the amorphous phase gradually undergo conformation changes and orient toward the fiber axis, creating an oriented noncrystalline phase. In the second region, the registry of the oriented molecules increases and some crystallization occurs.

The improved order in the crystalline phase leads to significant dipole−dipole interaction, resulting in the sudden shift in the frequency of the C═O vibration (small increase in density). In the last region, it is possible that the oriented noncrystalline and crystalline phases grow at the expense of the amorphous phase, resulting in a large increase in density with a limited increase in the in area fraction of the crystalline component of the C═O peak.

Care must be taken when comparing the results obtained on the drawn fibers with those obtained on the as-spun fibers. The different processing methods can results in vastly different sample morphologies. Thus, the degree of crystallinity for a specific density can be very different, which would result in different fractions of the C═O component bands.

Conclusion

The evolution of the morphology in a series of melt-spun PTT fibers was studied using polarized Raman spectroscopy. Three PTT films were first studied as standards to gain a better understanding of the origin of the different spectral features. By constructing a Raman spectrum for each sample in which the contribution of the molecular orientation has been removed, the bands that are representative of the crystalline phase or the amorphous phase were determined. The isolated carbonyl stretch at ∼1720 cm^{-1} showed significant variation with increasing crystallinity and was selected for a peak-fitting analysis. It was determined that the low-frequency component of the C═O band was representative of the crystalline phase. The frequency shift is believed to be due to dipole−dipole interactions that are possible only in the ordered crystalline phase.

The same analysis was then used to study the evolution of the morphology in the different fibers. It was determined that first an oriented noncrystalline phase was gradually developing as the sample density increased (increasing spin speeds and birefringence). For fibers having a density around 1.319 g/cm^3, the registry of the oriented molecules improved to the point that crystallization can suddenly occur, resulting in the shift in the frequency of the C═O stretching vibration.

The observations deduced from the carbonyl peak analysis were confirmed by the quantitative determination of the average molecular orientation. P_2 appears to increase linearly through the entire range of sample birefringence studied, supporting the previous conclusion regarding the creation of an oriented noncrystalline phase followed by crystallization. The simultaneous determination of P_4 allowed the determination of the orientation distribution function as a function of birefringence. Using P_2 and P_4 values calculated from functions fitted from the actual data, the ODF was plotted for the different birefringence values. The ODF results showed that the distribution of orientations of the C_1-C_4 axis of the benzene ring was growing along the fiber axis at low birefringence values but eventually appears to broaden around 0° instead of becoming narrower. These observations indicate that the molecules gradually get more ordered and in time resulting in a more defined orientation of the benzene rings. Eventually the molecules start to adopt the specific *tggt* conformation characteristic of the crystalline phase with the benzene rings oriented at 38°.

The determination of the terms directly dependent on the principal elements of the polarizability tensor showed a large variability as a function of birefringence. The variation of these molecular parameters may be explained using a two-phase model as suggested by the spectral analysis.

Finally, the peak analysis results obtained on drawn fibers were combined with those obtained on the as-spun fibers to observe the evolution of the sample morphology over a larger range of densities. The results showed that the evolution of the morphology in PTT fibers seem to followed three distinct regions as the sample density increases. First, an oriented noncrystalline phase is formed which results in a density increase. Suddenly, the order in the oriented noncrystalline phase improves resulting in significant crystallization. The regular chain arrangement in the crystalline phase results in strong dipole−dipole interaction of the C═O bonds, reducing the frequency of the stretching vibration. In the third region, both the oriented noncrystalline and the crystalline phases grow at the expense of the amorphous phase.

Acknowledgment. The authors acknowledge the NSF-DMR and DOE-PAIR for partial support of this work.

References and Notes

(1) Jakeways, R.; Ward, I. M.; Wilding, M. A.; Hall, I. H.; Desborough, I. J.; Pass, M. G. *J. Polym. Sci., Part B: Polym. Phys.* **1975**, *13*, 799−813.
(2) Ward, I. M.; Wilding, M. A.; Brody, H. *J. Polym. Sci., Part B: Polym. Phys.* **1976**, *14*, 263−274.
(3) Ward, I. M.; Wilding, M. A. *Polymer* **1977**, *18*, 327−335.
(4) Desborough, I. J.; Hall, I. H.; Neisser, J. Z. *Polymer* **1979**, *20*, 545−552.
(5) Poulindandurand, S.; Perez, S.; Revol, J. F.; Brisse, F. *Polymer* **1979,** *20*, 419−426.
(6) Kim, J. S.; Lewin, M.; Bulkin, B. J. *J. Polym. Sci., Part B: Polym. Phys.* **1986**, *24*, 1783−1789.
(7) Bulkin, B. J.; Lewin, M.; Kim, J. *Macromolecules* **1987**, *20*, 830−835.
(8) Pyda, M.; Boller, A.; Grebowicz, J.; Chuah, H.; Lebedev, B. V.; Wunderlich, B. *J. Polym. Sci., Part B: Polym. Phys.* **1998**, *36*, 2499−2511.
(9) Huang, J. M.; Ju, M. Y.; Chu, P. P.; Chang, F. C. *J. Polym. Res.* **1999**, *6*, 259−266.
(10) Huang, J. M.; Chang, F. C. *J. Polym. Sci., Part B: Polym. Phys.* **2000**, *38*, 934−941.
(11) Chisholm, B. J.; Zimmer, J. G. *J. Appl. Polym. Sci.* **2000**, *76*, 1296−1307.
(12) Ho, R. M.; Ke, K. Z.; Chen, M. *Macromolecules* **2000**, *33*, 7529−7537.
(13) Kim, K. J.; Bae, J. H.; Kim, Y. H. *Polymer* **2001**, *42*, 1023−1033.
(14) Lyoo, W. S.; Lee, H. S.; Ji, B. C.; Han, S. S.; Koo, K.; et al. *J. Appl. Polym. Sci.* **2001**, *81*, 3471−3480.
(15) Wu, J.; Schultz, J. M.; Samon, J. M.; Pangelinan, A. B.; Chuah, H. H. *Polymer* **2001**, *42*, 7141−7151.
(16) Grebowicz, J. S.; Brown, H.; Chuah, H.; Olvera, J. M.; Wasiak, A.; et al. *Polymer* **2001**, *42*, 7153−7160.
(17) Wu, J.; Schultz, J. M.; Samon, J. M.; Pangelinan, A. B.; Chuah, H. H. *Polymer* **2001**, *42*, 7161−7170.
(18) Wang, X. S.; Yan, D. Y.; Tian, G. H.; Li, X. G. *Polym. Eng. Sci.* **2001**, *41*, 1655−64.
(19) Jang, S. S.; Jo, W. H. *J. Chem. Phys.* **1999**, *110*, 7524−7532.
(20) Yang, J. S.; Jo, W. H. *J. Chem. Phys.* **2001**, *114*, 8159−8164.
(21) Yang, J.; Sidoti, G.; Liu, J.; Geil, P. H.; Li, C. Y.; Cheng, S. Z. D. *Polymer* **2001**, *42*, 7181−7195.
(22) Motori, A.; Saccani, A.; Sisti, L. *J. Appl. Polym. Sci.* **2002**, *85*, 2271−2275.
(23) Hong, P. D.; Chung, W. T.; Hsu, C. F. *Polymer* **2002**, *43*, 3335−3343.
(24) Chuah, H. H. *J. Polym. Sci., Part B: Polym. Phys.* **2002**, *40*, 1513−1520.
(25) Ramiro, J.; Eguiazabal, J. I.; Nazabal, J. *J. Appl. Polym. Sci.* **2002**, *86*, 2775−2780.
(26) Wu, G.; Li, H. W.; Wu, Y. Q.; Cuculo, J. A. *Polymer* **2002**, *43*, 4915−4922.
(27) Hong, P. D.; Chuang, W. T.; Yeh, W. J.; Lin, T. L. *Polymer* **2002**, *43*, 6879−6886.
(28) El Shafee, E. *Polymer* **2003**, *44*, 3727−3732.
(29) Kim, K. J.; Bae, J. H.; Kim, Y. H. *Polym. Int.* **2003**, *52*, 35−41.
(30) Pigeon, M.; Prudhomme, R. E.; Pezolet, M. *Macromolecules* **1991**, *24*, 5687−5694.
(31) Citra, M. J.; Chase, D. B.; Ikeda, R. M.; Gardner, K. H. *Macromolecules* **1995**, *28*, 4007−4012.
(32) Lesko, C. C. C.; Rabolt, J. F.; Ikeda, R. M.; Chase, B.; Kennedy, A. *J. Mol. Struct.* **2000**, *521*, 127−136.
(33) Yang, S.; Michielsen, S. *Macromolecules* **2002**, *35*, 10108−10113.
(34) Bower, D. I. *J. Polym. Sci., Part B: Polym. Phys.* **1972**, *10*, 2135−2153.
(35) Purvis, J.; Bower, D. I.; Ward, I. M. *Polymer* **1973**, *14*, 398−400.
(36) Everall, N. *Appl. Spectrosc.* **1999**, *53*, 461A-A.
(37) Frisk, S.; Ikeda, R. M.; Chase, D. B.; Rabolt, J. F. *Appl. Spectrosc.* **2004**, *58*, 279−286.
(38) Frisk, S.; Ikeda, R. M.; Chase, D. B.; Rabolt, J. F. *Appl. Spectrosc.* **2003**, *57*, 1053−1057.
(39) Bower, D. I. *J. Phys. B: At., Mol. Opt. Phys.* **1976**, *9*, 3275−3293.
(40) Lewis, E. L. V.; Bower, D. I. *J. Raman Spectrosc.* **1987**, *18*, 61−70.
(41) Bower, D. I. *J. Polym. Sci., Part B: Polym. Phys.* **1981**, *19*, 93−107.
(42) Pottel, H.; Herreman, W.; Vandermeer, B. W.; Ameloot, M. *Chem. Phys.* **1986**, *102*, 37−44.
(43) Yang, S.; Michielsen, S. *Macromolecules* **2003**, *36*, 6484−6492.
(44) Melveger, A. J. *J. Polym. Sci., Part A2: Polym. Phys.* **1972**, *10*, 317.
(45) Bulkin, B. J.; Lewin, M.; Deblase, F. J. *Macromolecules* **1985**, *18*, 2587−2594.
(46) Rodriguez-Cabello, J. C.; Quintanilla, L.; Pastor, J. M. *J. Raman Spectrosc.* **1994**, *25*, 335−344.

MA049234J